1 **Bisphenol-S removal via photoelectro-Fenton/H$_2$O$_2$ process using Co-**
2 **Porphyrin/Printex L6 gas diffusion electrode**

3

4

5

6

7 **Paulo Jorge Marques Cordeiro-Junior[1,2]*• Alysson Stefan Martins[1]• George**
8 **Bueno Santana Pereira[3] • Fillipe Vieira Rocha[3]• Manuel Andrés Rodrigo Rodrigo[2,*]•**
9 **Marcos Roberto de Vasconcelos Lanza[1,*]**

10

11 [1] São Carlos Institute of Chemistry, University of São Paulo (USP), Trabalhador São-
12 carlense street 400, 13566-590, São Carlos, SP, Brazil

13 [2] Department of Chemical Engineering, Universidad de Castilla-La Mancha, Campus
14 Universitario s/n, 13071 Ciudad Real, Spain

15 [3] Department of Chemistry, Federal University of São Carlos (UFSCar), Rodovia
16 Washington Luiz km 235, 13565-905, São Carlos, SP, Brazil
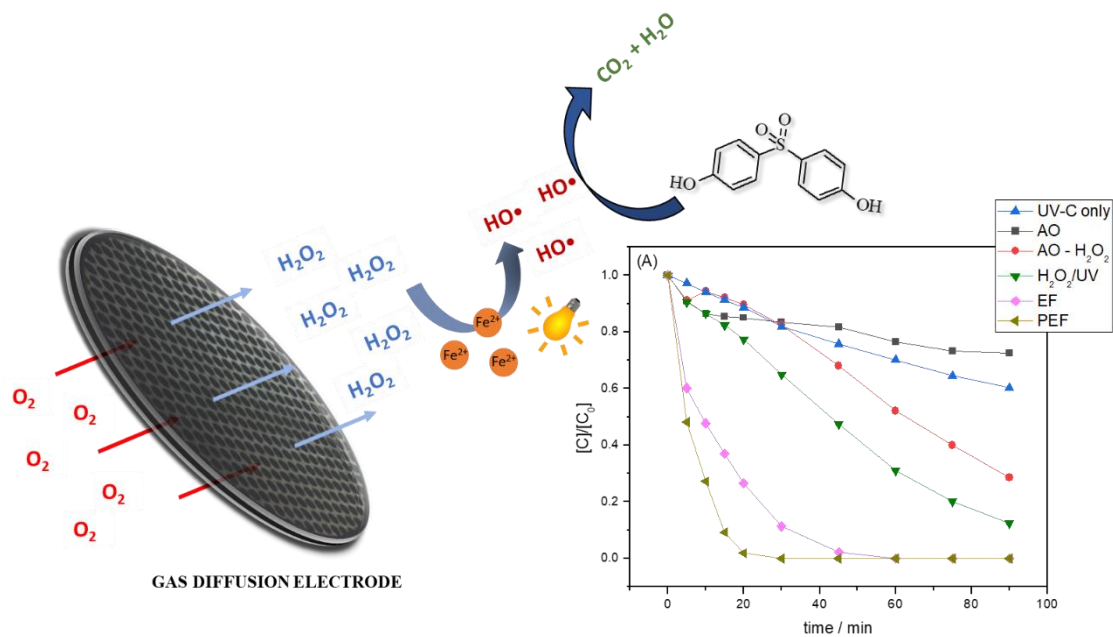
17

18

19

20

21

22

23

24

25

26

27

28

29

30 *Corresponding authors: Manuel.Rodrigo@uclm.es (Manuel Andrés Rodrigo Rodrigo)
31 pjmcjunior@usp.br (Paulo J. M. Cordeiro-Junior)
32 marcoslanza@usp.br (Marcos R. de Vasconcelos Lanza)

GRAPHICAL ABSTRACT

ABSTRACT

1

2   The present work reports the development and application of gas diffusion electrode

3   (GDE) based on carbon Printex L6 modified with 5% Co-Porphyrin/CPL6 for the

4   removal of Bisphenol S (BPS) in wastewater using different electrochemical advanced

5   oxidation processes (EAOPs). The application of the modified GDE led to the in-situ

6   generation of 333 mgL^{-1} of H_2O_2 in only 90 min; this represents an increase of 88% in

7   H_2O_2 generation in relation to the unmodified GDE. The process involving bisphenol S

8   degradation fitted well into a pseudo-first order kinetic reaction for all the treatment

9   techniques evaluated; the treatment techniques investigated recorded an increase in

10 kinetic rate constant in the following order: anodic oxidation (0.004 min^{-1}) < UV-C (0.006

11 min^{-1}) < H_2O_2 (0.008 min^{-1}) < H_2O_2/UV-C (0.016 min^{-1}) < electro-Fenton (0.063 min^{-1})

12 < photo electro-Fenton (0.154 min^{-1}). The photo electro-Fenton (PEF) process exhibited

13 the best degradation efficiency; BPS was completely removed after only 30 min of

14 treatment and 78% mineralization was recorded after 360 min of treatment. The

15 remaining organic matter under the PEF treatment process corresponded to short-chain

16 carboxylic acids; this confirms the efficiency of the process applied for BPS

17 decontamination. The results obtained show that the proposed treatment mechanism can

18 be successfully combined with cheaper biological treatments for a total remediation of

19 wastes.

20

21 **Keywords:** Bisphenol-S; electrochemical advanced oxidation processes; hydrogen

22 peroxide; gas diffusion electrode.

23
24
25
26

1   **1. Introduction**

2   Endocrine disruptors (ED) are a group of organic compounds that cause damages

3   to the endocrine system of living beings, undermining the proper functioning of this

4   system. ED may cause interferences in the body system of animals (fish, birds, reptiles

5   and mammals) during hormone biosynthesis, metabolism, or hormonal activity,

6   compromising their reproductive system of animals [1,2]. In some marine species, the

7   exposure to ED can compromise the immune and nervous systems of these species and

8   change the phenotypes of male fish. Similarly, human exposure to ED can cause several

9   diseases including endometriosis and hormone-dependent cancers, such as testicular,

10   prostate, and breast cancers [1–3]. A wide range of chemicals have been found to act as

11   ED; among these chemicals include anthropogenic substances, such as phthalates,

12   alkylphenols, organochlorines, bisphenols, parabens, biphenyls polychlorides, pesticides,

13   and pharmaceutical and natural substances, such as estrogens and phytoestrogens [1,2].

14   Although the negative effects of EDs are very well known, many of these

15   substances, such as the bisphenols are still widely employed in the production of diverse

16   plastic products (which are among the chemicals with the highest production volume

17   worldwide) [4–6]. Human exposure to the bisphenols has been linked to several

18   pathologies, with particular emphasis to chronic diseases, including cardiovascular

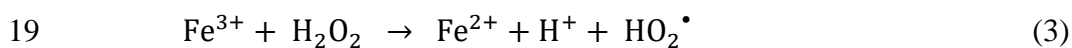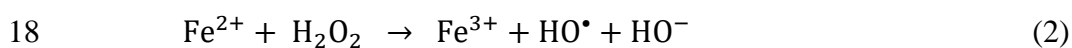19   problems and type-2 diabetes [5,6].

20   Bisphenol-S (BPS), also referred to as 4,4'-sulfonyldiphenol [$(C_6H_4OH)_2SO_2$], is

21   a white crystalline solid at room temperature which is highly soluble in water. BPS is

22   commonly used as the main reagent in the production of polycarbonate and epoxy resins.

23   Due to its excellent stability at high temperatures and resistance to sunlight, and especially

24   to the less rigid regulations, BPS is used as a substitute for bisphenol-A (BPA) [7,8]. The

25   products containing BPS in their composition are often dubbed "BPA-free".

1   Interestingly, contrary to BPA, there are scarce data in the literature regarding the toxic

2   and long-term effects of BPS. Furthermore, the structural similarity of BPA and BPS

3   makes it essentially important to conduct comprehensive comparative analyses targeted

4   at investigating the effects of BPS on the endocrine system [8,9].

5   Previous studies have shown that BPS can affect the fertility of female mice, even

6   when administered at sub-chronic exposure levels [10,11]. Very few studies reported in

7   the literature have compared the action mechanism of BPA and BPS. One of these works

8   that merits attention is the study conducted by Maćczak A. et al. (2017) which showed

9   that BPS exhibits substantial oxidative potential in red blood cells compared to BPA;

10   according to the findings of this study, BPS affects human organism via acute poisoning

11   or through occupational exposure [12]. BPS can cause disruption in the endocrine system

12   by affecting endocrine properties through its interaction in the human estrogen alpha

13   receptor, leading to a significant reduction in the body's testosterone secretion [10,13].

14   Considering the widespread use of BPS as a substitute for BPA in several industries,

15   significant concentrations of BPS have increasingly been identified in surface water,

16   groundwater, sewage water, and in drinking water; in view of that, there have been

17   growing concerns regarding the toxic effects of BPS on humans, animals and the

18   environment as a whole [13,14]. In the USA, there has been a sharp rise in mean BPS

19   contamination since it started to be evaluated [7]. In China, the presence of BPS has been

20   confirmed in lakes and rivers affected by extreme pollution from industrial waste

21   discharge [15,16]. In an attempt to assess human exposure to BPS, Liao (2012)

22   biomonitored urine in several Asian countries; the author detected the presence of BPS

23   in approximately 81% of the samples investigated [8,9].

24   Studies on the removal of BPS in water/wastewater through the application of

25   alternative treatments are still scarce in the literature. The traditional treatment methods

1 (including physicochemical or biological treatment techniques) employed for the removal

2 of this kind of contaminants in water/wastewater have been found to be largely inefficient

3 in degrading/removing molecules with recalcitrant characteristics found in low

4 concentrations. Thus, considering the risk of contamination and the continuous

5 emergence of new pollutants that act as endocrine disruptors, the scientific community

6 has sought to explore innovative, low cost and sustainable treatment techniques that are

7 capable of ensuring the safety removal of these contaminants from the aquatic

8 environment. In recent years, advanced oxidation processes (AOPs) have gained

9 prominence over conventional treatment methods; this is because AOPs have been found

10 to be capable of degrading most hazardous organic compounds, transforming them into

11 CO_2, H_2O, or inorganic anions [17,18]. AOPs are primarily based on the generation of

12 hydroxyl radical (•OH), which is an oxidative agent that has high reactivity ($E^o = 2.8$ V

13 vs EPH – standard hydrogen electrode). One of the precursors of hydroxyl radical is

14 hydrogen peroxide (H_2O_2); this product can be combined with UV radiation (Eq 1) or can

15 be made to react with Fe^{2+}, giving rise to Fenton or photo-Fenton processes (Eq 2-4)

16 [18,19].

17 $$H_2O_2 \xrightarrow{h\nu} 2\ HO^\bullet \tag{1}$$

18 $$Fe^{2+} + H_2O_2 \rightarrow Fe^{3+} + HO^\bullet + HO^- \tag{2}$$

19 $$Fe^{3+} + H_2O_2 \rightarrow Fe^{2+} + H^+ + HO_2^\bullet \tag{3}$$

20 $$Fe^{3+} + HO_2^\bullet \rightarrow Fe^{2+} + H^+ + O_2 \tag{4}$$

21

22   One way to improve the Fenton-based processes is through coupling with

23 electrochemical methods, so-called electrochemical advanced oxidation processes

(EAOPs) [19–22], which are based on the destruction of the organic compounds by anodic oxidation and/or by in situ generation of H_2O_2 at the cathode. H_2O_2 can be produced by the oxygen reduction reaction (ORR) via two-electron transfer at a carbonaceous cathode ($E^0 = 0.68$ V vs SHE), according to the Eq 5 [19–22].

$$O_2 + 2\,H^+ + 2\,e^- \rightarrow H_2O_2 \qquad\qquad (5)$$
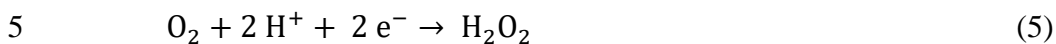
Another advantage of EAOPs is that Fe^{2+} can be quickly and continuously regenerated by reduction of Fe^{3+} at the cathode ($E^0 = 0.77$ V vs SHE), according to Eq 6 [20,22].

$$Fe^{3+} + e^- \rightarrow Fe^{2+} \qquad\qquad (6)$$

The use of gas diffusion electrodes (GDE) allows the electrogeneration of H_2O_2 in high concentrations through ORR. GDEs are composed of an amorphous carbon black matrix and an agglomerating agent known as polytetrafluorethylene (PTFE); these materials form a multichannel structure which allows the flow of oxygen and partial penetration of solution in the device. Previous studies reported in the literature have shown that Printex L6 carbon is one of the best cathodic materials for the electrogeneration of H_2O_2 in ORR via 2 e⁻ [23,24]. However, the application of this cathodic material (Printex L6 carbon) in ORR leads to high energy consumption – thus, energy consumption is one of the limiting factors of the reaction. In this sense, the modification of Printex L6 carbon matrix with energy-saving materials is an alternative approach that has been widely employed with a view to reducing the amount of energy consumed in the ORR process, without affecting the efficiency of the materials. Coordinated compounds, such as cobalt (II) porphyrins, have been shown to be an excellent modifier of Printex L6 carbon when it comes to obtaining high concentrations of H_2O_2.

The present work investigates the use of a GDE containing Printex L6 carbon modified with 5.0 % Co-Porphyrin for the degradation of Bisphenol-S. The modified GDE was employed toward the degradation and mineralization of Bisphenol-S using different AOPs, including photolysis (UV-C) and anodic oxidation (AO), and combined processes involving H_2O_2 electrogeneration, such as AO-H_2O_2, AO-H_2O_2/UV-C, electro-Fenton (FE), and photo-electro-Fenton (PEF) processes. The byproducts generated from BPS oxidation were further evaluated under optimized degradation conditions.

2. Experimental

2.1 Chemical

Printex L6 carbon was purchased from Evonik Ltd. (Brazil). The following reagents were used to perform the assays: isopropyl alcohol (Vetec, 99.5%), potassium sulfate (Sigma-Aldrich, 99%), sulfuric acid (Vetec, 97.8%), 60% w/w poly (tetrafluoroethylene) dispersion (PTFE – Uniflon), ammonium molybdate (Sigma-Aldrich, 99%), iron (II) sulfate heptahydrate (Synth, 99%), Bisphenol S (AlfaAesar, 99%), and Acetonitrile (Vetec, 99%). The aqueous solutions were prepared using ultrapure water (Milli-Q system with resistivity >18 MΩ cm).

2.2   Synthesis of Co-Porphyrin

Porphyrin was synthesized based on the methodology described by Momo et al. [25]. For the synthesis of Co-Porphyrin, 0.14 mmol of porphyrin was solubilized in dimethylformamide (DMF), and 0.7 mmol of Cobalt precursor (Co(CH$_3$CO$_2$)$_2$.4H$_2$O) was added into the mixture. The synthesized mixture was kept under reflux and in inert atmosphere for 90 minutes. After filtration, the residue was removed using chloroform and water. The organic layer was dried under vacuum with anhydrous Na$_2$SO$_4$ until the

1 solvent was reduced to 3 mL. The Co-Porphyrin compound was crystallized with hexane

2 to obtain a purple solid.

3 ### 2.3 Fabrication and electrochemical study of GDEs

4 For the construction of the unmodified GDE, 8 g of the catalytic mass (previously

5 dried) containing amorphous carbon Printex L6 and 40% (w/w) of the hydrophobic

6 binding agent (PTFE) were used. In the case of the GDE modified with 5.0 % Co-

7 Porphyrin, the respective amount (w/w) of Co-Porphyrin was added to the carbon Printex

8 L6 matrix. The catalytic mass was added between two wire mesh stainless steel perforated

9 uniformly, and the material was subjected to heating (at 290 °C) and pressing (at 7.5 ton)

10 for 2 hours.

11 Electrochemical studies of the modified GDE (GDEm) and unmodified GDE

12 (GDE) were carried out in order to determine the amount of H_2O_2 produced in an

13 undivided electrochemical cell (coated with a thermostatic bath at 25 ºC) composed of

14 the working electrode (GDE and GDEm), a platinum counter electrode, and Ag/AgCl 3M

15 - used as reference electrode, as can be seen in Figure S1. The working electrode is located

16 at the bottom of the electrochemical cell secured by a flange coupled with a system with

17 O_2 gas connection. This compartment is constantly pressurized to 0.2 bar of O_2 gas. The

18 pressure of 0.2 bar of the O_2 gas is already widely used in other studies by our research

19 group [26–28], and this is the optimal condition used, since it constantly keeps the GDE

20 saturated with oxygen. And so, the limitation of mass transfer by O_2 is eliminated.

21 Electrolysis was carried out using the following constant potentials: -0.50, -1.00,

22 -1.50, -1.75, -2.00, -2.25, -2.50 V, for 90 minutes. Supporting electrolyte: 0.1 mol L^{-1} of

23 K_2SO_4 at pH = 2.5, adjusted with H_2SO_4. The amount of electrogenerated H_2O_2 was

1   quantified by UV-Vis absorption spectrophotometry (λ=350 nm) using ammonium

2   molybdate solution (2.4×10^{-3} mol L^{-1}).

3   **2.4 BPS degradation via EAOPs using modified GDE**

4   The electrochemical experiments involving BPS degradation were performed

5   based on the set-up previously described. An aqueous solution containing 50 mg L^{-1} of

6   BPS and 0.1 mol L^{-1} K_2SO_4, at pH 2.5, was used to perform the degradation analysis. A

7   constant potential of -1.50 V vs Ag/AgCl was applied for 90 min at a temperature of 25

8   ºC. The degradation assays were performed using the following EAOPs: (i) anodic

9   oxidation (AO); (ii) UVC light only; (iii) anodic oxidation via H_2O_2 electrogeneration

10   with GDE (AO-H_2O_2); (iv) anodic oxidation via H_2O_2 electrogeneration with GDE under

11   UVC light (AO-H_2O_2-UVC); (v) electro-Fenton process (EF); and (vi) photo-electro-

12   Fenton process (PEF). The UVC irradiation source employed was as follows:

13   monochromatic Pen-Ray mercury lamp (model 11SC-2.12_90-0012-01) at 254 nm and

14   4,750 mWcm^{-2}. For the EF and PEF assays, $FeSO_4.7H_2O$ 0.10 mmol was used as a source

15   of Fe^{2+}.

16   Prior to performing the analyses, all collected samples were filtered with a 25 mm

17   x 0.45 um Xtra Pet chromatil filter (diameter x pore size). BPS was monitored in the

18   assays by high-performance liquid chromatography (HPLC) using a Shimadzu 20A LC

19   system coupled to UV/Vis detector (254 nm). The analyses were performed using a

20   Varian C18 column (5.0 μm; 250×4.60mm i.d.) eluted isocratically at a flow rate of 0.6

21   mL min^{-1} with 60:40 acetonitrile/water (v/v) at 40 ºC and injection volume of 20 µL. The

22   mineralization of BPS was monitored through total organic carbon analysis (TOC) using

23   a Shimadzu analyzer model TOC-VCPN. The rate (in percentage terms) of mineralization

24   was calculated using equation (7), where TOC_0 stands for the initial concentration value

25   of BPS at time 0 and TOC is the concentration value of BPS at a specific time t.

$$TOC\ removal\ (\%) = \frac{(TOC_0 - TOC)}{TOC_0} x100\% \hspace{2cm} (7)$$

The following equipment was used for quantifying the organic acids formed during the degradation process: ion chromatography system - 174 model 850 Professional IC, coupled to a 940 Professional IC module 175 (Metrohm) with a 580 IC conductimetric detector. The IC-column employed: Metrosep Organic acids 250/7.8 mm model from Metrohm; mobile phase: 0.075 mol L^{-1} H_2SO_4; flow rate: 0.5 mL min^{-1}; oven temperature: 60 ºC; and injection volume: 20 µL. The BPS-derived aromatic intermediates were identified by LC-MS TOF 6230 (model Agilent 1260 Infinity) with an electrospray interface operating under the following conditions: ion polarity mode as negative, nebulizer at 50 psi, drying gas at 10.0 L min^{-1}, gas temperature at 325°C, VCap of 3500 V and skimmer voltage of 65 V. Analysis was performed using a Zorbax Eclipse Plus C-18 column (4.6 mm × 100 mm; 3.5 µm) at a flow rate of 0.15 mL min^{-1} with 70:30 acetonitrile:water and injection volume of 5 µL.

3. Results and discussion

3.1 Electrogeneration of H_2O_2 by GDEm and mechanisms

The results obtained from the electrolysis performed at constant potentials of -0.50, -1.00, -1.50, -1.75, -2.00, -2.25, -2.50 V vs Ag/AgCl for the modified and unmodified GDEs are shown in Figure 1. As can be observed, the maximum concentration of H_2O_2 (after 90 min) obtained for the GDE modified with 5% Co-Porphyrin was higher under practically all the potentials evaluated. The unmodified GDE recorded higher H_2O_2 concentration only at potentials superior to -2.25 V. This observation is evident when one looks at the ratio of H_2O_2 concentration between the GDEm and the GDE. The modified GDE exhibited approximately 7.8, 1.55 and 0.88-fold

1   increase in H_2O_2 electrogeneration compared to the unmodified GDE for the first three

2   potentials investigated.

3   The application of the GDEm yielded maximum concentration of H_2O_2 at -1.75

4   V, with 340 mg L^{-1} of H_2O_2 electrogenerated. However, one notices a constant baseline

5   of H_2O_2 generation starting at -1.5 V (with 333 mg L^{-1} of H_2O_2 generated). This shows

6   that, in terms of cost-benefit analysis, the potential of -1.5 V offers the best relationship

7   between H_2O_2 generation and energy cost; this is because, at this potential, there is only

8   a slight increase in H_2O_2 production when the potential is increased. The application of

9   the unmodified GDE yielded maximum H_2O_2 concentration at -2.25 V, with 301 mg L^{-1}

10   of H_2O_2 electrogenerated. At -1.5 V, the unmodified GDE produced H_2O_2 concentration

11   of 177mg L^{-1}; this represents a decrease of 53 % in the amount of H_2O_2 generated by the

12   modified GDE.

13   The Co-Porphyrin/CPL6 displaces the beginning of the ORR to more positive

14   values, and thus, obtain a greater electrogeneration of H_2O_2 at lower over potentials (< -

15   2.0 V vs Ag/AgCl). However, the catalyst Co [29,30], like other metals such as Zr [31],

16   Cu [30], Pd, Nb and Mo [32], not only displaces the ORR, but also parallel reactions,

17   such as the hydrogen evolution reaction - HER ($2H^+ + 2e^- \rightarrow H_2$). At high values of

18   potential, the HER has a strong influence on the carbonaceous materials. In this way, as

19   part of the current intensity is destined to this parasitic reaction, the high efficiency to

20   H_2O_2 generation of GDEm is lost. The same effect will be observed for the unmodified

21   GDE for potentials greater than -2.25 V, which it is possible to observe the decay in the

22   maximum H_2O_2 electrogeneration with the improvement of potential applied.

23   Other parallel reactions are the reduction of H_2O_2 to H_2O molecule via 2-electron

24   transfer ($H_2O_2 + 2H^+ + 2e^- \rightarrow H_2O$) on the surface of the cathode and the oxidation of

25   H_2O_2 to O_2 on the anode ($H_2O_2 \rightarrow O_2 + 2H^+ + 2e^-$). Both reactions have more intensity

1 when high concentrations of H_2O_2 are present ($[H_2O_2] > 300$ mg L^{-1} for both electrodes)

2 depending on the electrochemical cell settings.

3   Thus, the loss of H_2O_2 can be attributed to these effects, thus, for GDEm it occurs

4 at lower potential values than for GDE. For this reason, GDEm presented lower values of

5 electrogenerated H_2O_2 compared to GDE at potentials -2.25 and -2.5 V vs Ag/AgCl.
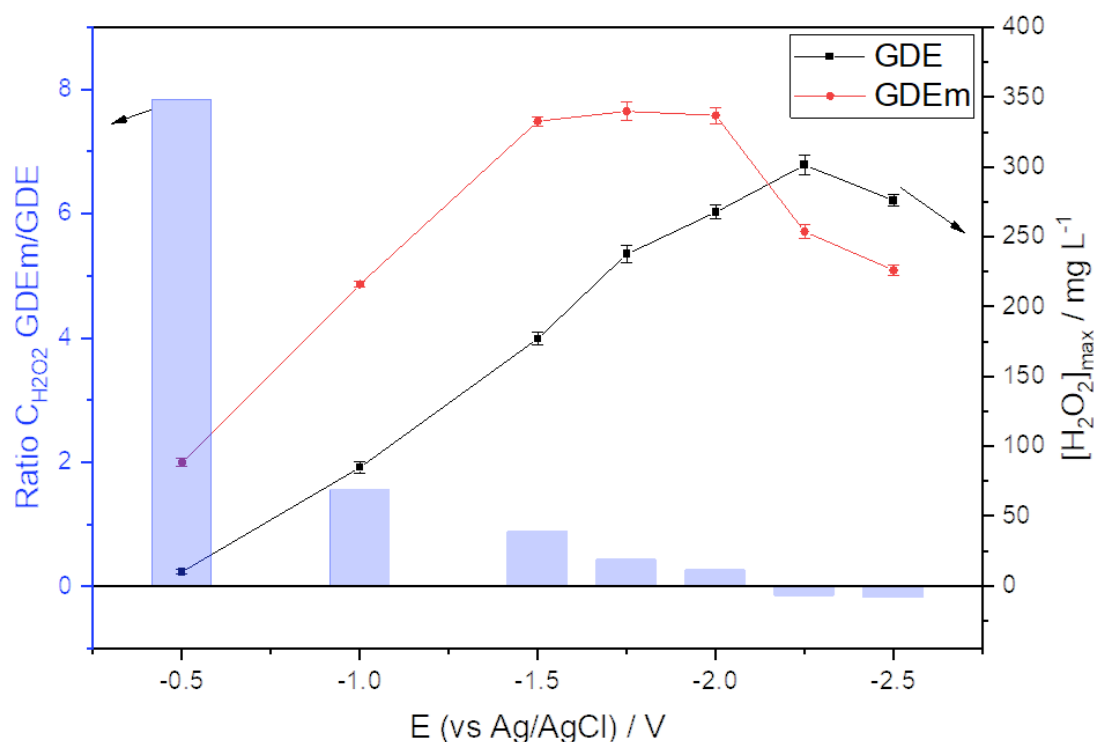
7 **Figure 1.** Correlation of maximum H_2O_2 electrogenerated (mg L^{-1}) and the ratio of GDEm/GDE
8 in terms of H_2O_2 concentration in 90 min of electrolysis under applied constant potentials of -
9 0.50, -1.00, -1.50, -1.75, -2.00, -2.25 and -2.50 V vs Ag/AgCl 3M. Supporting electrolyte
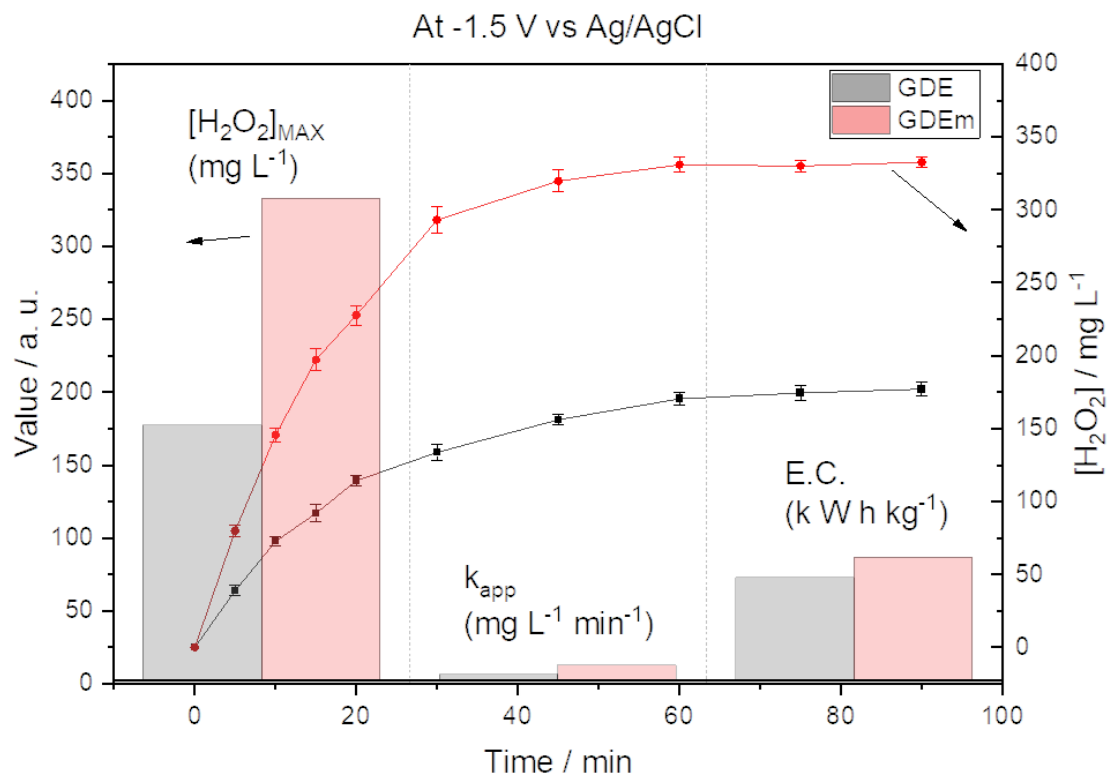10 employed: 0.1 mol L^{-1} K_2SO_4 at pH 2.5.

12   Figure 2 shows the values of H_2O_2 concentration obtained from the electrolysis

13 performed at -1.5 V. One will observe that both the GDEm and the GDE exhibited a linear

14 increase in H_2O_2 generation up to 20 min of electrolysis; this result showed that the ORR

15 process was characterized by a kinetic reaction of pseudo-zero order, since the O_2

16 concentration was the limiting factor for the occurrence of ORR. The modified GDE

1   exhibited a K_{app} value of 12.49 mg L^{-1} min^{-1}, which was approximately twice the value

2   obtained for the unmodified GDE (6.11 mg L^{-1} min^{-1}).

3   A comparative analysis was performed regarding energy consumption (E.C.) in

4   kWh kg^{-1} based on the application of the modified GDE and unmodified GDE at the

5   potential of -1.50 V; E.C was calculated using equation (8) below, where E stands for the

6   cell potential (in V), I is the current (in A), t is the time (in h), V is the volume (in L) and

7   [H_2O_2] is the H_2O_2 concentration in 90 min (in mg L^{-1}).

8        $$E.C(kWh\ kg^{-1}) = \frac{1000\ EIt}{V\ [H_2O_2]} \qquad\qquad (8)$$

9   Figure 2 shows the results obtained from the analysis of energy consumption

10   (E.C.) based on the application of electrolysis at constant potential of -1.50 V. As can be

11   observed, the unmodified GDE exhibited E.C value of 72.5 kWh kg^{-1}, while the modified

12   GDE presented relatively higher E.C of 86.6kWh kg^{-1}. While the energy consumption

13   value obtained for the modified GDE was slightly higher than that of the unmodified

14   GDE, the amount of hydrogen peroxide produced under the application of the modified

15   GDE was much higher compared to that obtained from the unmodified GDE.

Figure 2. Electrogeneration of H_2O_2 based on the application of the unmodified GDE (GDE) and modified GDE (5.0 % Co-Porphyrin/CPL6) – GDEm, at the potential of -1.50 V vs Ag/AgCl 3M, using 0.1 mol L^{-1} K_2SO_4, at pH 2.5, as supporting electrolyte. The bar graph shows a comparative analysis of the GDEm and the GDE in terms of the following: kinetic constant (mg L^{-1} min^{-1}); energy consumption (kWh kg^{-1}); and maximum H_2O_2 concentration generated (mg L^{-1}).

Compared to the unmodified GDE, the higher efficiency of the modified GDE in terms of H_2O_2 generation can be attributed to the synergistic effect observed in the processes involving the formation of H_2O_2. Considering that GDE is composed of amorphous carbon materials - Printex L6 carbon in this case, its structure contains oxygenated functional groups such as quinones and carboxylic acids; these functional groups influence the displacement of the electronic density of the neighboring carbon, thus making it an active site for ORR, as represented in Figure 3 and in equation 5.
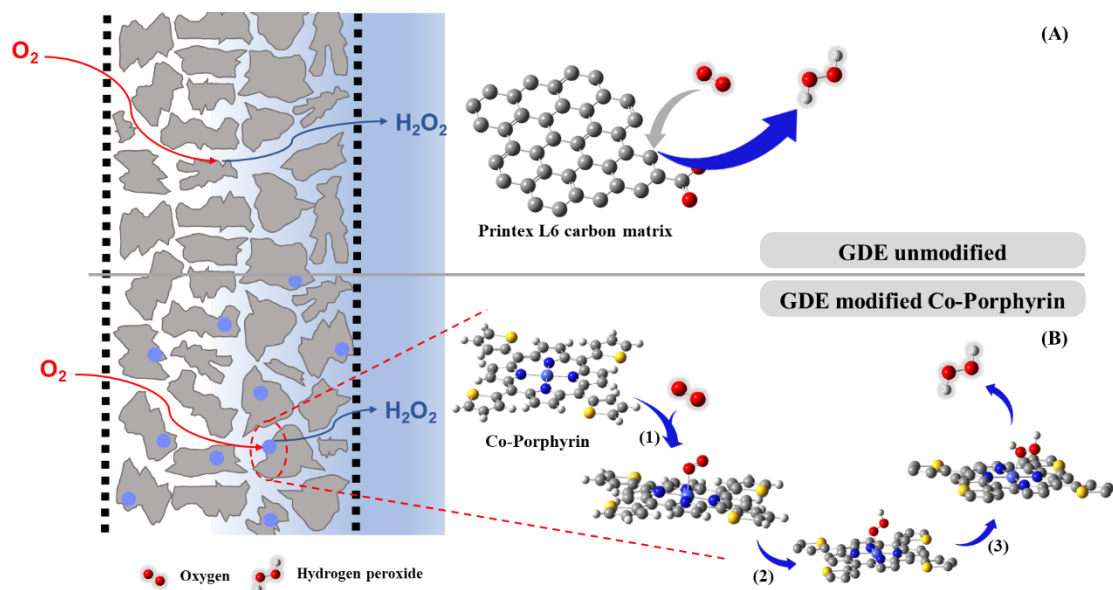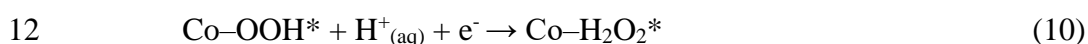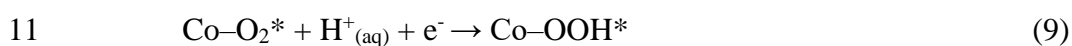
15

Figure 3. Illustration of the catalytic effects of oxygen reduction reactions that occur in both GDEs: **(A)** - unmodified GDE and **(B)** - modified GDE (5.0 % Co-Porphyrin/CPL6). Steps: (1) $O_{2(g)} + ^* \rightarrow O_2^*$; (2) $O_2^* + H^+ + e^- \rightarrow HOO^*$; (3) $HOO^* + H^+ + e^- \rightarrow H_2O_2^*$.

The major problem regarding the use of unmodified GDE has to do with the high overpotentials required for the ORR to occur, which leads to high energy consumption. Thus, the modification of GDE with coordinated compounds – such as porphyrin compounds, helps reduce the energy costs involved in the process. Some previous studies have already pointed out cobalt (II) metal as one of the most selective materials when it comes to performing ORR via 2 e^- [30,33].
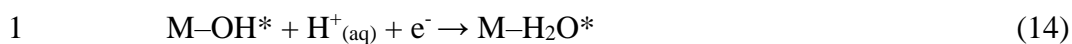
Under the conditions that were employed in our experimental assays, the O_2 gas is highly saturated either as dissolved in the aqueous medium or flowing through the multichannel structure of GDEm. In this way, the use of these types of electrodes eliminates the low O_2 solubility, since the gas is continuously injected directly to the GDE under a pressure of 0.2 bar, thus, the reagents of ORR are renewed into the three-phase surface of the electrode [28]. Hence, the O_2 will be sufficiently available to interact both with the Co metal and with the active sites of the Printex L6 carbon matrix and thus electrochemically generate the H_2O_2.

1   The O_2 adsorption mechanism in the cobalt (II) metallic center is directly

2   interconnected to the successive reaction steps involved in the process. The first step,

3   which is based on the Pauling model, involves the interaction of O_2 with Co through a

4   simple single chemical bond (Co–O=O*). One will note that although there are two other

5   models that can be employed in this step – namely, the Griffith and Ponte models, none

6   of them tend to form H_2O_2 as their final product (instead, the application of these two

7   models leads to the formation of H_2O). The formation of the intermediate state Co–O=O*

8   is followed by the formation of the adsorbed species Co–OOH* from the transfer of one

9   electron and H^+. The formation of H_2O_2 can occur through this reaction according to

10   equations 9 to 11 and as illustrated in Figure 3B.

11          $Co–O_2* + H^+_{(aq)} + e^- \rightarrow Co–OOH*$ (9)

12          $Co–OOH* + H^+_{(aq)} + e^- \rightarrow Co–H_2O_2*$ (10)

13          $Co–H_2O_2* \rightarrow H_2O_{2(aq)}$ (11)

14   Considering that the great complexity of ORR lies in the fact that the process can

15   lead to the formation of H_2O_2 via $2e^-$ or H_2O via $4e^-$, the crucial step involves the

16   formation of the intermediate state M–OOH*. The metallic center acts by removing or

17   donating electronic density of this intermediate species, depending on the number of

18   electrons present in its valence shell; thus, this exerts influence over which pathway the

19   ORR will take. If there is a strong interaction, the time of permanence of the species

20   *OOH will be long enough for the formation of the intermediate species HO* and O* to

21   occur; hence, the H_2O molecule will be generated as the final product (equations 12-14).

22          $M–OOH* \rightarrow M–O* + M–HO*$ (12)

23          $M–O* + H^+_{(aq)} + e^- \rightarrow M–HO*$ (13)

1 $$M\text{–}OH^* + H^+_{(aq)} + e^- \rightarrow M\text{–}H_2O^* \tag{14}$$

2 According to Baran et al. [33], the metallic center Co (II) is the most favorable catalyst

3 for ORR via 2e-, since the M–OOH* interaction tends to follow the reaction described in

4 equation 9. This is because the energy values between cobalt and the *OH and *O species

5 are no ideal; this implies the absence of interaction between the metal (cobalt) and the

6 intermediates. According to Baran et al [33], this M-OOH* trend (whose reaction tends

7 to generate H_2O_2) is observed from left to right in the periodic table, with the metal Co

8 being the most efficient in this sequence. Thus, Co-OOH* metal presents the ideal Gibbs

9 free energy values to stabilize this chemical transition state (and, consequently, lead to

10 the formation of H_2O_2), compared to other intermediates (Co-OH* or Co-O*), whose

11 Gibbs free energy are less likely to occur with metal Co. Other metals, in turn, have ideal

12 Gibbs free energy values for the formation of M-OH* or M-O* states, and thus, are more

13 efficient catalysts for the generation of H_2O_2, such as Ni or Cu.

14 In addition, a third synergistic effect is also observed only in the modified GDE;

15 this effect is related to the influence of the amorphous carbon matrix in the Co-Porphyrin

16 complex. The huge amount of conjugated π electrons that the Printex L6 carbon possesses

17 in its structure interacts with the complex through the π–π stacking [34]; this helps in the

18 stabilization of the Co metallic center with the intermediate species *OOH, and,

19 consequently, facilitates the generation of H_2O_2.

20 **3.2 Degradation of BPS by EAOPs using GDEm**

21 The efficiency of BPS (50 mg L^{-1}) degradation process was evaluated through

22 different EAOPs (H_2O_2; H_2O_2/UV; EF and PEF) via H_2O_2 electrogeneration using GDE

23 modified with 5% Co-Porphyrin/CPL6 in a batch reactor. For comparison purposes, the

24 following treatment processes were also carried out in the same conditions: photolysis –

1   PT (using UV-C irradiation only) and anodic oxidation (AO) under N_2 gas flow. Figure

2   4 (A) shows the results obtained from the degradation of BPS as a function of time. As

3   can be noted, the lack of H_2O_2 electrogeneration under the AO and PT processes led to

4   low degradation efficiency, with only 20% and 30% of BPS removal, respectively. This

5   low oxidation rate is reasonable in the sense that the degradation process occurs only via

6   direct oxidation on the platinum counter-electrode under the AO process and via direct

7   photodecomposition of BPS under the PT process, which shows significant photo

8   resistance.
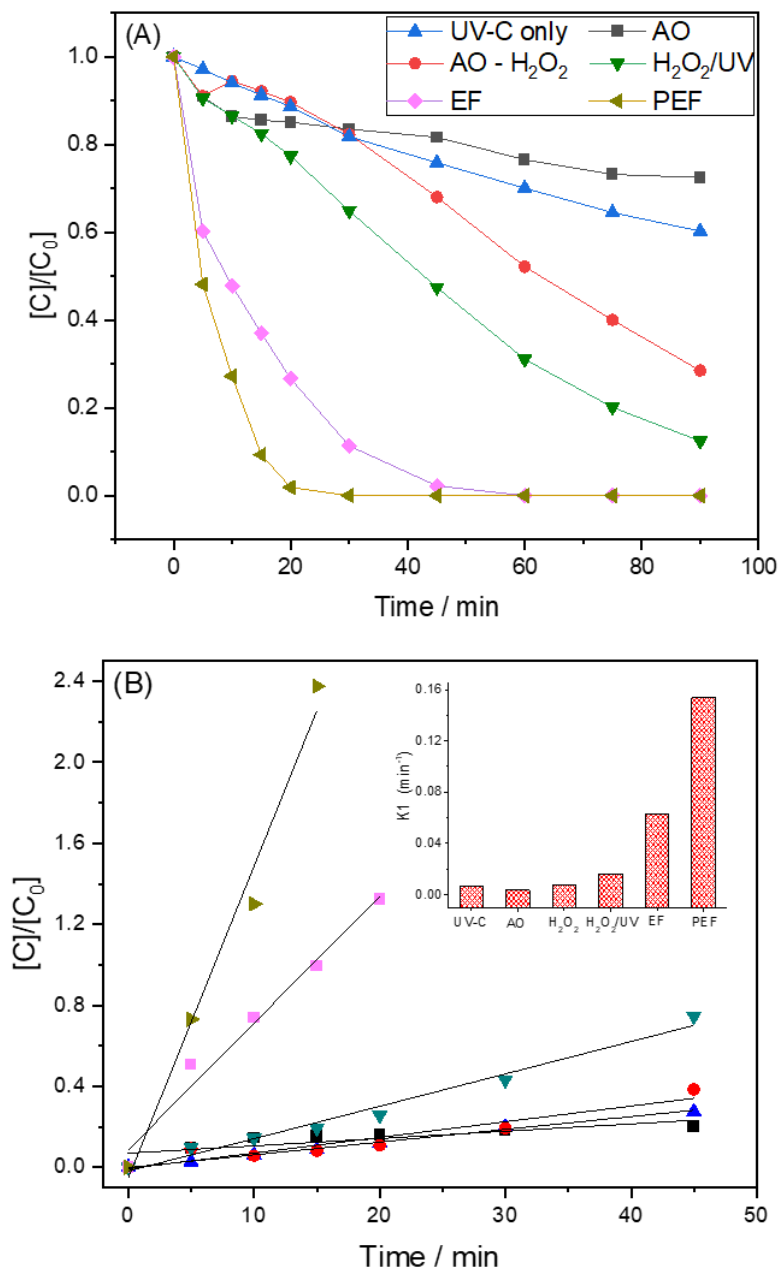
1
2 **Figure 4.** **(A)** BPS removal (50 mg L^{-1}) and **(B)** analysis of pseudo-first order kinetics based on
3 the application of different EAOPs using GDE modified with 5.0 % Co-Porphyrin/CPL6 at bias
4 potential of -1.50 V vs Ag/AgCl; supporting electrolyte: 0.1 mol L^{-1} K$_2$SO$_4$ at pH = 2.5. EAOPs
5 evaluated: UV-C Only; AO; AO-H$_2$O$_2$; AO-H$_2$O$_2$/UVC EF and PEF. The inset shows the
6 corresponding pseudo-first-order kinetic constant.
7

8   The efficiency of the process involving BPS degradation increases substantially

9 when H$_2$O$_2$ is electrogenerated in the oxidation process. The improvement in BPS

10 degradation is attributed to the oxidation capacity of •OH generated in high concentration

11 from H$_2$O$_2$. The application of the AO-H$_2$O$_2$ and H$_2$O$_2$/UV treatment processes resulted

12 in 70% and 80% of BPS removal within 90 min of treatment, respectively. The slightly

20

1   greater improvement observed under the H_2O_2/UV process is associated with the

2   additional •OH generated from H_2O_2 photolysis in the bulk solution.

3   The application of the electro-Fenton process led to the complete removal of BPS

4   (> 99%) within 60 min of reaction. This great performance is mainly attributed to the

5   action of Fe^{2+} as a catalyst. Precisely, Fe^{2+} increases the amount of •OH radical produced

6   in the solution medium (Eq. 2-4). Fe^{2+} is regenerated by direct electron transfer on the

7   cathode (Eq. 3 and 6). The combination of UV irradiation with electro-Fenton gives rise

8   to photo electro-Fenton (PEF) process; the application of the PEF process for BPS

9   degradation further enhanced the degradation efficiency, and BPS was completely

10   removed after 30 min of treatment. The excellent oxidation rate observed under the PEF

11   process stems from the synergistic effect of the electro-Fenton reactions and the

12   photolysis from UV light; this combination promotes the formation of more •OH radicals

13   and enhances BPS degradation [19,35]. The kinetic constant curves obtained are shown

14   in Figure 4 (B). As can be observed (Fig. 4 (B), BPS removal was well-fitted into a pseudo

15   first-order kinetic equation; this indicates a constant production of •OH radicals for the

16   oxidation of BPS molecules. As shown in the inset of Figure 4(B), the k_1 value obtained

17   for the PEF process (0.154 min^{-1}) was approximately 2.5 and 10-fold higher compared to

18   the value recorded for the EF and H_2O_2/UV processes, respectively; this points to the

19   excellent performance of the combination of the electro-Fenton technique with UV light.

20   The H_2O_2 concentrations during the degradation assays for the AO-H_2O_2,

21   H_2O_2/UV, EF and PEF processes using GDEm can be seen in Figure S2(A). The profile

22   highlighted in the black line refers to the electrolysis to electrogeneration of H_2O_2 at the

23   potential of -1.5 V vs Ag/AgCl which it was used for comparation (no presence of BPS).

24   It can be observed that the most efficient degradation processes had lower values of

25   electrogenerated H_2O_2, since part of the generated peroxide is converted with hydroxyl

1 radicals. In Figure S2(B), the residual H_2O_2 values at 90 min and the estimated amount

2 of H_2O_2 activated to •OH (based on electrolysis at -1.5 V without the target compound)

3 are shown. PEF, whose process is the most efficient for the conversion of H_2O_2 to •OH,

4 compared to the EF, H_2O_2/UV and AO-H_2O_2, presented the lowest value of H_2O_2,

5 reaching, at the end of 90 min, the residual value of 196.41 mg L^{-1} and therefore, around

6 135.6 mg L^{-1} of activated H_2O_2. The conversion rate of H_2O_2 to •OH was estimated for

7 each process based on the value obtained in electrolysis at -1.5 V in 90 min (332 mg L^{-1}

8 ^{1}), with values of 5.8; 8.0; 22.4 and 40.8% for the AO-H_2O_2, H_2O_2/UV, EF and PEF

9 processes respectively.

10   To evaluate the removal of organic matter, TOC measurements were carried, and

11 these measurements were compared with the energy consumption for all the EAOPs

12 investigated. The energy consumption (EC) was estimated based on Equation (15) [36],

13 where E_{cel} is the cell potential (V), I is the current of the system (A), t is the time employed

14 in the EAOP treatment (h), and ΔTOC is the mass of total organic carbon removed (kg).

15 $$EC = \frac{i.E_{cel}.t}{\Delta TOC} \qquad\qquad (15)$$

16 As can be seen in Figure 5, TOC removal was found to be directly proportional to the

17 BPS oxidation rate (Fig. 4). Although 30% of BPS molecules were oxidized under the

18 photolysis process, the organic matter remained practically constant (< 1% TOC

19 removal); this points to the photostability of the by-products after the photooxidation of

20 BPS. The electrolysis processes, namely, AO, AO-H_2O_2, and AO-H_2O_2/UV, promoted a

21 considerable improvement in oxidation with similar mineralization rates (of ~12%).

22 Under these processes (AO, AO-H_2O_2, and AO-H_2O_2/UV), the organic matter is oxidized

23 via a direct mechanism under the AO process and via an indirect mechanism through the

24 action of H_2O_2 molecules under the AO-H_2O_2 and AO-H_2O_2/UV processes, and by UV-

1　　light under the AO-H$_2$O$_2$/UV process. However, one will note that the oxidation

2　　efficiency of these processes was still low due to the low oxidizing power of the

3　　electrogenerated H$_2$O$_2$. As a result, the EC values obtained for the AO-H$_2$O$_2$ and AO-

4　　H$_2$O$_2$/UV processes were relatively high (9.78 and 7.08 kWh kg^{-1}, respectively), as shown

5　　in the inset of Figure 5. Although the combination of radiation source and H$_2$O$_2$ was

6　　expected to promote a better performance in terms of TOC removal, the by-products

7　　appeared to be more resistant to oxidation compared to the BPS molecule; as such, the

8　　rate of mineralization was slightly lower than expected. With regard to the AO process

9　　performed under N$_2$ flow, the EC value recorded was very low; this is found to be

10　reasonable since there were no reactions involving ORR for H$_2$O$_2$ generation under this

11　process, and, as such, there was a significant drop in the cathodic current (see Figure 5-

12　inset).
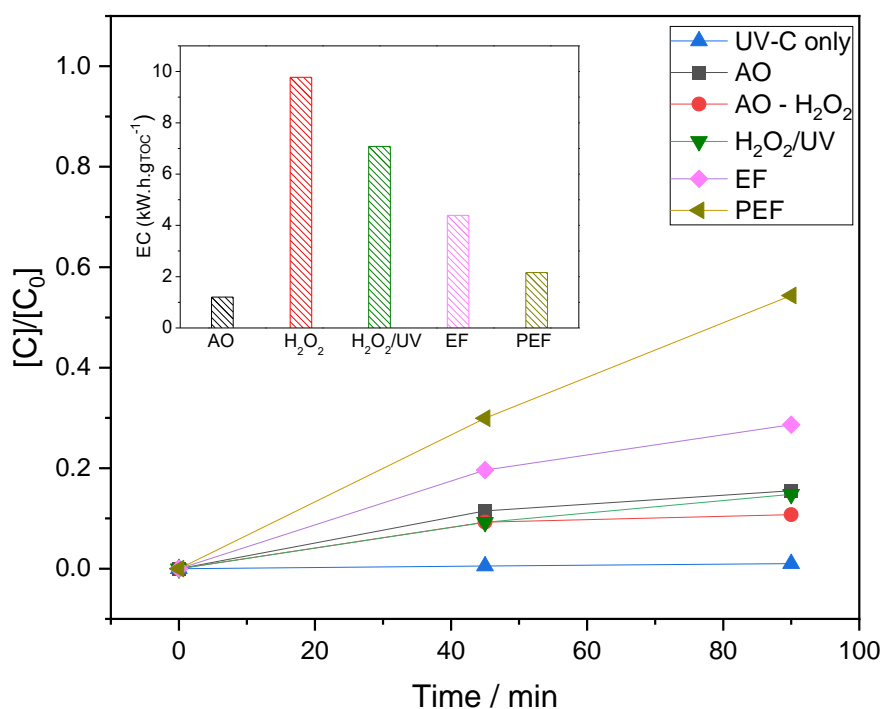
13
14　**Figure 5.** TOC mineralization for the degradation of BPS (50 mgL^{-1}) based on the application of
15　different EAOPs. Conditions applied: E=-1.50 V vs Ag/AgCl; supporting electrolyte: 0.1 mol L^{-1}
16　K$_2$SO$_4$ at pH = 2.5; and UV-C light. EAOPs applied: UV-C Only; AO; AO-H$_2$O$_2$; AO-H$_2$O$_2$/UVC
17　EF and PEF. Inset: Energy consumption (EC) under the electrochemical processes employed.
18

1   The application of the electro-Fenton (EF) and photo electro-Fenton (PEF)

2   processes yielded the best mineralization rates and promoted complete oxidation of BPS

3   in less than 60 min of treatment. However, the PEF process was found to be more efficient

4   in terms of mineralization; this process yielded 55% of TOC removal - which was twice

5   the mineralization rate obtained under the EF process. In view of that, the PEF process

6   recorded a significant drop in EC (4.38 kWh kg^{-1}) compared to the EF process (1.96 kWh

7   kg^{-1}). These results point to the importance of the combined application of electro-Fenton

8   with UV irradiation when one seeks to obtain maximum degradation efficiency in terms

9   of the oxidation of both BPS molecules and the by-products.

10   Based on these results, the photo electro-Fenton (PEF) technique was found to be

11   the most suitable EAOP for the treatment of BPS.

12   To obtain the highest mineralization rate, the reaction time was further evaluated.

13   Figure 6A shows the results obtained from a comparative analysis of energy consumption

14   (EC) and TOC removal under the application of the PEF technique for 360 min. As

15   expected, an increase in the treatment period resulted in an increase in the rate of

16   mineralization. An approximately 67% TOC conversion was recorded within 180 min of

17   degradation and the highest mineralization was recorded after 360 min of treatment (~

18   80%); these results point to the excellent performance of the PEF process. It is worth

19   noting that while there was a progressive increase in EC with the increase of the treatment

20   period, the increase in the rate of mineralization justified the increase in energy

21   consumption. A further observation that deserves mentioning is that, under the PEF

22   technique, the EC required for performing 6 hours of treatment (6.26kWh kg^{-1}) was only

23   ~30% higher than the EC required to perform 1 hour of treatment via the EF technique;

24   in addition, the EC required to perform 6 h of treatment under the PEF technique

25   (6.26kWh kg^{-1}) was lower than the EC required to perform 1 h of treatment under the

1 H_2O_2 and H_2O_2/UV techniques (9.77 and 7.07 kWh kg^{-1}, respectively). These results

2 clearly point to the efficiency and superiority of the PEF treatment technique over the

3 other treatment techniques evaluated in this study. In short, the application of the PEF

4 technique promoted the greatest efficiency in BPS degradation, with low energy

5 consumption compared to the other techniques.

6   Our results show that the energy required to degrade the BPS compound with

7 ~78% mineralization was 6.26 kWh kg^{-1} in 6 hours of PEF treatment. Comparing with

8 other techniques employed in the electrochemical degradation of BPS via AOP that were

9 recently reported in the literature, our findings showed lower values of energy

10 consumption. For example: i) Vasconcelos et al, 2020, studied the electrochemical

11 oxidation of BPS using $Ti/Ru_{0.25}Ir_{0.25}Ti_{0.5}O_2$ anodes produced by microwave-assisted

12 hybrid heating method, which are characterized by having a low cost, high catalytic

13 activity and high durability. The EC for the treatment via anodic oxidation was 211 kWh

14 kg^{-1}, obtaining mineralization values around 20% in only 60 min at 100 $mAcm^{-2}$ [37]. ii)

15 the study by Zhang et al (2020), whose electrochemical oxidation of BPS was performed

16 employing Nd-Doped PdO_2 anodes, reaching BPS removal values around 95% at a

17 current density of 15 mA cm^{-2} with energy consumption values equal to 60.26 and 95.45

18 kWh m^{-3} using Ti/PdO_2-Nd and Ti/PdO_2 anodes in 60 min of treatment [38]. Both CE

19 value are much higher than that obtained in the present study. Until now, no studies

20 employing the PEF degradation of BPS have been reported. However, in order to compare

21 the energy consumption via PEF processes employing GDE, degradation studies with

22 other target contaminants were reported. Lima et al 2020, employed unmodified GDE in

23 the degradation of ciprofloxacin via PEF treatment. In 360 min, the energy consumption

24 was 9.81 kWh kg^{-1} to mineralize ~85% of ciprofloxacin [39]. Kronka et al (2020), using

25 a GDE modified with 1.0% of 1,4-naphthoquinone in the paracetamol drug degradation

1   via PEF treatment at 75 mA cm^{-2} for 180 min obtained an EC value of 6.35 kWh kg^{-1} and

2   42% of mineralization [27]. As can be seen, unmodified or modified GDE applied in

3   treatment processes via PEF have lower energy consumption values compared to other

4   techniques used in EAOP. It is worth mentioning that each compound has its degree of

5   complexity to degrade and/or mineralize, thus, the examples cited are just to get an idea

6   of the energy consumption of GDE in general.

7

8
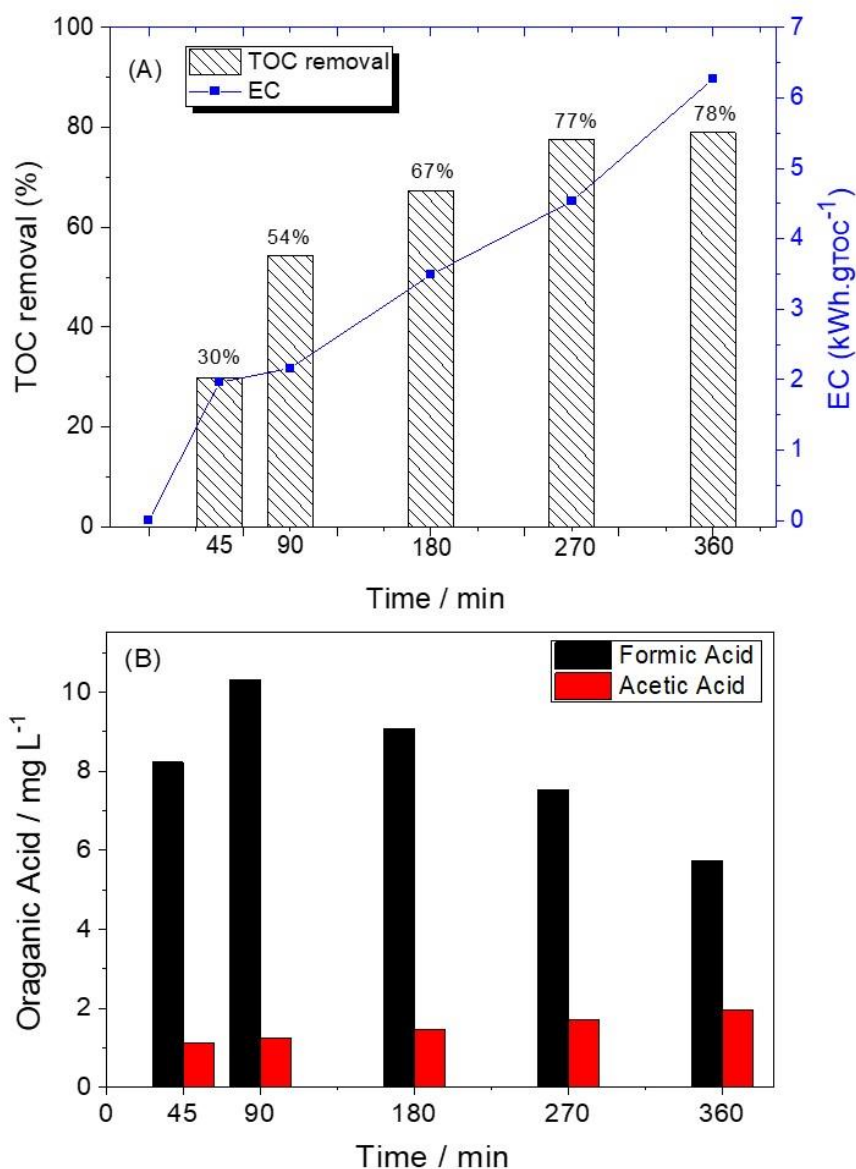
9
10 **Figure 6. (A)** Comparative analysis of TOC mineralization and energy consumption as a function
11 of time; and **(B)** evolution of the concentration of the final oxidation intermediates - acetic acid

and formic acid, in BPS degradation (50 mgL^{-1}) through the PEF process. Conditions applied: E=-1.50 V vs Ag/AgCl; supporting electrolyte: 0.1 mol L^{-1} K$_2$SO$_4$ at pH = 2.5; and UV-C light.

It should be noted that the mineralization rate was practically constant in the last hour of treatment. This outcome is attributed to the generation of recalcitrant molecules during the oxidation of BPS; these molecules were found to be more resistant to the treatment process. Thus, ion chromatography analysis was performed in order to investigate the intermediates generated during the decomposition of BPS. The presence of formic acid, oxalic acid and acetic acid was confirmed as major reaction intermediates in the process. According to previous studies reported in the literature [40–42], bisphenol compounds (BPX) can experience •OH radical attack during the initial stage of the reactions, and this leads to the generation of BPX derivatives which are oxidized to one-ring aromatic compounds. The subsequent oxidation of these intermediates leads to the formation of short aliphatic carboxylic acids like oxalic acid, formic acid, and acetic acid. Eventually, a portion of these acids is converted into CO$_2$, H$_2$O, and inorganic ions. Figure 6B shows the concentration of formic acid and acetic acid (intermediates) generated in relation to time; oxalic acid was detected only qualitatively. The concentration of formic acid can be found to increase over time and then decreases after 180 min of treatment, with a 40% reduction at the end of the treatment. Interestingly, the concentration of acetic acid exhibits a slight increase throughout the experimental periods; this result shows that most of the acetic acid consumed in the process is completely mineralized, while a chunk of the remaining portion is converted to formic acid. It is worth pointing out that although a small amount of organic matter remained at the end of the treatment process, a greater portion of this material was converted to short-chain aliphatic carboxylic acids with low toxicity. These results help confirm the excellent degradation efficiency of the PEF technique when it comes to the decontamination of BPS. The combined application of the

1 PEF process with cheaper biological treatment processes is a highly efficient and less

2 costly technique that can be employed toward the total remediation of wastes.

3.3 Identification of intermediaries and proposed degradation pathway

4 The aromatic organic intermediates that were generated during the BPS

5 degradation assays via PEF for 360 min at 1.5 V vs Ag/AgCl were analyzed by LC-MS.

6 Table 2 summarizes the identified degradation intermediates and the exact values of their

7 respective masses during PEF degradation.

8 Six BPS-derived intermediates were identified, which is the main pathway of •OH

9 attack, by hydroxylation. The degradation pathway is initiated by the hydroxylation of

10 BPS to yield the intermediates 4-(4-hydroxybenzene-1-sulfonyl)benzene-1,2-diol (**1**),

11 4,4'-sulfonyldi(benzene-1,2-diol (**2**) and/or 4,4'-sulfonyldi(benzene-1,2-diol) (**3**). The

12 intermediate (**1**) can be undergo to further hydroxylation steps to produce the

13 intermediates (**2**) or (**3**) or 3,4-dihydroxy benzene-1-sulfonic acid (**4**). Intermediate (**3**)

14 can be degraded via 2 pathways: the first with formation of the hydroquinone molecule;

15 or with formation of the intermediary (**4**), followed by the formation of the catechol. In

16 both pathways, the final product is the benzene-1,2,4-triol. The subsequent steps are the

17 opening of the aromatic ring to yield the open chain organic intermediates, until reaching

18 the total mineralization into CO_2, H_2O and SO_4^{2-}. The proposed mineralization pathway

19 for bisphenol S via the PEF process is shown in Figure 7. Some of BPS-derived

20 intermediates reported in this work were also identified by the authors Zhang et al [38]

21 and Luo et al [43], via electrochemical oxidation of BPS. Zhang et al, reported only

22 aromatic intermediates of higher mass with structures similar to intermediates (1) and (2);

23 However, Luo et al., whose mineralization efficiency reached values of approximately

24 26% in 120 min, could identify compounds such as: intermediate (4) and hydroquinone.

1 It is worth mentioning that the efficiency of the PEF processes, due to the synergism of

2 the continuous electrosynthesis of H_2O_2 coupled with UVC radiation, regeneration of Fe^{2+}

3 ions and anodic oxidation, results in a high generation of •OH in the solution, and

4 consequently, by-products decomposed of BPS from low mass are obtained, as well as

5 higher mineralization rates.

6

7

8 **Table 1.** Summary of the identified aromatic intermediates of BPS by LC-MS during the PEF
9 degradation for 360 min at 1.5 V vs Ag/AgCl

Name / Abbreviation	Formula	m/z	Feasible structure
BPS	$C_{12}H_{10}O_4S$	250.0299	
(1)	$C_{12}H_{10}O_5S$	266.0249	
(2)	$C_{12}H_{10}O_6S$	282.0198	
(3)	$C_6H_6O_4S$	173.9987	
(4)	$C_6H_6O_5S$	189.9936	

Hydroquinone	$C_6H_6O_2$	110.0368	
Catechol	$C_6H_6O_2$	110.0368	
1,2,4-Benzenetriol	$C_6H_6O_3$	126.03169	

1

2

3

Figure 7. Proposed BPS mineralization pathway by PEF degradation for 360 min at 1.5 V vs Ag/AgCl.

6

3.4 Leakage of Co ions from GDEm

Cobalt has both beneficial effects on human health (composed of vitamin B12 or cyanocobalamin) and harmful [44–47]. The International Agency for Research on Cancer (IARC) classifies cobalt as a possible human carcinogen, being its main source of contamination through the respiratory system causing cancer of the lung or adrenal gland [45]. According to the study reported by Ortega et al, 2014, particles of low-solubility cobalt oxides are readily incorporated by lung cells, causing acute toxicity [48]. Contamination by the accumulation of cobalt in water or soil can affect the fruit or seed ecosystems of plants that grow in contaminated environments, which are later sources of food for humans. Cobalt can be found in the environment from natural sources such as rocks, soils (0.1 – 50 ppm), plants (0.1 – 2 ppm), animals and in surface water (0.1 – 10 µg/L) or sea water (0.01 – 4 µg/L), or human activities through mining or industrial processes [44–47].

Thus, it is clear that cobalt ion has non-negligible impacts on the environment and human health. And consequently, the environmental impacts that it could cause if it were to be leached from the GDEm into water is a concern that we have to keep in mind. The cobalt ion leakage from the GDEm was investigated by cyclic voltammetry.

The leakage of the Co-Porphyrin catalyst from the Printex L6 carbon matrix was evaluated by cyclic voltammetry technique (CV) [24,26] employing a rotating ring-disc electrode (RRDE-Pine Instrument – AFE7R9GCPT) as working electrode, Pt-counter electrode and Ag/AgCl (KCl 3 mol L^{-1}). A dispersion containing 2.5 mg of the material in 1 ml of dimethylformamide was prepared; and 25 µL of this solution was dropped onto the electrode disc. VC analysis was performed over a potential range from +0.8 to -0.6 V, scan speed of 50 mVs^{-1} per 100 cycles using a Potenciostat/Gasvanostat Autolab PGSTAT-128N equipment, controlled by the Nova software.

1   In figure 8, it is possible to see the VC profile of both materials (CPL6 and Co-

2   Porphyrin/CPL6). The Co-Porphyrin/CPL6 catalyst does not present any redox peaks

3   regarding the metal transition, this often occurs when the Printex L6 carbon matrix is

4   employed, which due to its high capacitive current masks the possible peaks of the cobalt

5   complex. The evident reduction peak refers to the ORR which for the CPL6 (unmodified)

6   occurs at a potential of -0.3 V and for Co-Porphyrin/CPL6 it occurs at a potential of +0.1

7   V. In addition, from the first to the hundredth cycle there is no change in the CV profile

8   with increase of the cycles. Also, no changes were observed in the current value at the

9   peak of reduction as the number of cycles increases, suggesting that there is no leakage

10 of Co or CPL6 from the electrode.
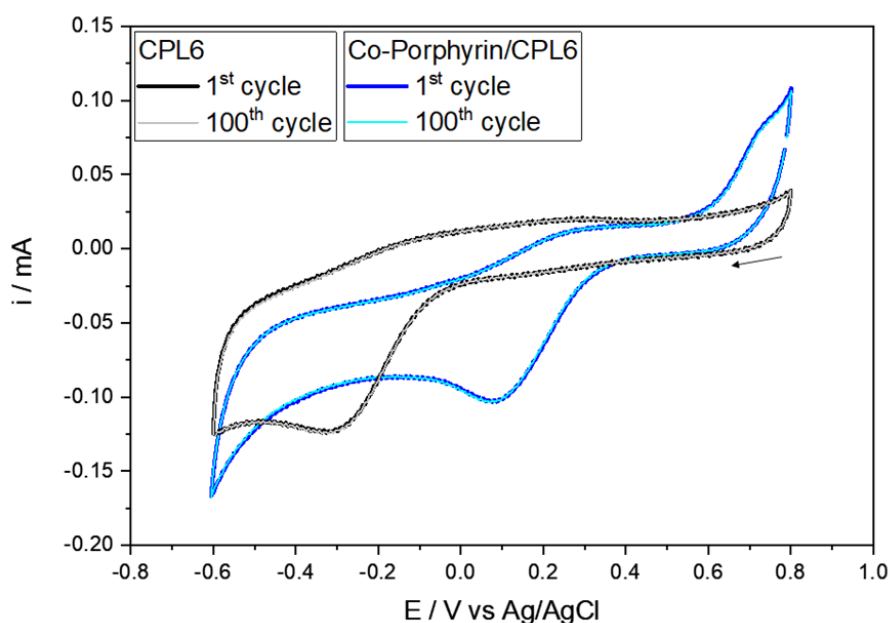
11

12 **Figure 8.** Cyclic voltammogram for the CPL6 (black line) and Co-Porphyrin/CPL6 (blue
13 line) recorded at 50 mV s^{-1}, using 0.1 mol L^{-1} K$_2$SO$_4$ at pH 2.5 as supporting electrolyte.

14

15   It is worth mentioning that the catalysts normally used in GDE must be insoluble

16 in water, as is the case with the Co-porphyrin complex. Furthermore, during the synthesis

17 of the catalytic mass (Co-Porphyrin + CPL6 + PTFE), PTFE agglomerates both materials

18 in a very homogeneous and stable way, so that the leakage of both materials is very

1   difficult. However, as a way to analyze a possible leakage of Co^{2+} ions from the GDE,

2   the solutions used before and after an electrolysis assays at -1.5 V for 360 min were

3   quantified, as well as after the BPS degradation test via PEF. As can be seen in table S1,

4   Co values were not found in the solution. Only values for Fe^{2+} were found for the

5   solutions before and after the degradation tests.

6

7   **CONCLUSION**

8   The present work reported the development of gas diffusion electrodes based on

9   amorphous carbon Printex L6 modified with 5.0 % Co-Porphyrin/CPL6 for the

10   electrogeneration of H_2O_2 and the application of these electrodes for the degradation of

11   Bisphenol S. The following conclusions can be drawn from the results obtained in this

12   study:

13   • The application of the modified GDE promoted an in-situ generation of

14   333 mg L^{-1} of H_2O_2 under the applied potential of -1.50 V vs Ag / AgCl

15   3M in only 90 min of treatment; this represents an increase of 88% in H_2O_2

16   electrogeneration compared to the amount of H_2O_2 generated under the

17   application of the unmodified GDE.

18   • A comparative analysis of different EAOPs showed that the photo electro-

19   Fenton (PEF) process exhibited the greatest efficiency in terms of BPS

20   degradation. Under the PEF process, BPS was completely removed after

21   30 min of treatment, and the process promoted mineralization rates of 67%

22   in 180 min and 80% in 360 min of treatment, with energy consumption of

23   3.49 and 6.26 kWh kg^{-1}, respectively.

- The remaining organic matter after the PEF process corresponds to short-chain carboxylic acids; this result helps confirm the efficiency of the PEF process in the decontamination of BPS. Furthermore, the successful application of the PEF process in combination with cheaper biological treatment processes can lead to the total remediation of wastes.

ACKNOWLEDGEMENTS

L

REFERENCES

[1] S.A. Snyder, P. Westerhoff, Y. Yoon, D.L. Sedlak, Pharmaceuticals, Personal Care Products, and Endocrine Disruptors in Water: Implications for the Water Industry, 2003.

[2] P. Westerhoff, Y. Yoon, S. Snyder, E. Wert, Fate of endocrine-disruptor, pharmaceutical, and personal care product chemicals during simulated drinking water treatment processes, Environmental Science and Technology. 39 (2005) 6649–6663. https://doi.org/10.1021/es0484799.

[3] M.M. Cook, E.M. Symonds, B. Gerber, A. Hoare, E.S. van Vleet, M. Breitbart, Removal of six estrogenic endocrine-disrupting compounds (EDCs) from

municipal wastewater using aluminum electrocoagulation, Water (Switzerland). 8 (2016). https://doi.org/10.3390/w8040128.

[4]   W. Qiu, H. Zhan, J. Hu, T. Zhang, H. Xu, M. Wong, B. Xu, C. Zheng, The occurrence, potential toxicity, and toxicity mechanism of bisphenol S, a substitute of bisphenol A: A critical review of recent progress, Ecotoxicology and Environmental Safety. 173 (2019) 192–202. https://doi.org/10.1016/j.ecoenv.2019.01.114.

[5]   B.A. Rocha, L.F. Azevedo, M. Gallimberti, A.D. Campiglia, F. Barbosa, High Levels of Bisphenol A and Bisphenol S in Brazilian Thermal Paper Receipts and Estimation of Daily Exposure, Journal of Toxicology and Environmental Health - Part A: Current Issues. 78 (2015) 1181–1188. https://doi.org/10.1080/15287394.2015.1083519.

[6]   Z. Fang, Y. Gao, X. Wu, X. Xu, A.K. Sarmah, N. Bolan, B. Gao, S.M. Shaheen, J. Rinklebe, Y.S. Ok, S. Xu, H. Wang, A critical review on remediation of bisphenol S (BPS) contaminated water: Efficacy and mechanisms, Critical Reviews in Environmental Science and Technology. 50 (2020) 476–522. https://doi.org/10.1080/10643389.2019.1629802.

[7]   S. Eladak, T. Grisin, D. Moison, M.-J. Guerquin, T. N'Tumba-Byn, S. Pozzi-Gaudin, A. Benachi, G. Livera, V. Rouiller-Fabre, R. Habert, A new chapter in the bisphenol A story: bisphenol S and bisphenol F are not safe alternatives to this compound, Fertility and Sterility. 103 (2015) 11–21. https://doi.org/10.1016/j.fertnstert.2014.11.005.

[8]   C. Liao, F. Liu, K. Kannan, Bisphenol S, a new bisphenol analogue, in paper products and currency bills and its association with bisphenol a residues, Environmental Science and Technology. 46 (2012) 6515–6522. https://doi.org/10.1021/es300876n.

[9]   C. Liao, F. Liu, H. Alomirah, V.D. Loi, M.A. Mohd, H.B. Moon, H. Nakata, K. Kannan, Bisphenol S in urine from the United States and seven Asian countries: Occurrence and human exposures, Environmental Science and Technology. 46 (2012) 6860–6866. https://doi.org/10.1021/es301334j.

[10] Z. Zhang, L. Lin, Y. Gai, Y. Hong, L. Li, L. Weng, Subchronic bisphenol S exposure affects liver function in mice involving oxidative damage, Regulatory Toxicology and Pharmacology. 92 (2018) 138–144. https://doi.org/10.1016/j.yrtph.2017.11.018.

[11] A. Nourian, A. Soleimanzadeh, A.S. Jalali, G. Najafi, Effects of bisphenol-S low concentrations on oxidative stress status and in vitro fertilization potential in mature female mice, 2017.

[12] A. Maćczak, M. Cyrkler, B. Bukowska, J. Michałowicz, Bisphenol A, bisphenol S, bisphenol F and bisphenol AF induce different oxidative stress and damage in human red blood cells (in vitro study), Toxicology in Vitro. 41 (2017) 143–149. https://doi.org/10.1016/j.tiv.2017.02.018.

[13] C. Héliès-Toussaint, L. Peyre, C. Costanzo, M.C. Chagnon, R. Rahmani, Is bisphenol S a safe substitute for bisphenol A in terms of metabolic function? An in vitro study, Toxicology and Applied Pharmacology. 280 (2014) 224–235. https://doi.org/10.1016/j.taap.2014.07.025.

[14] R. Viñas, C.S. Watson, Bisphenol S disrupts estradiol-induced nongenomic signaling in a rat pituitary cell line: Effects on cell functions, Environmental Health Perspectives. 121 (2013) 352–358. https://doi.org/10.1289/ehp.1205826.

[15] H. Jin, L. Zhu, Occurrence and partitioning of bisphenol analogues in water and sediment from Liaohe River Basin and Taihu Lake, China, Water Research. 103 (2016) 343–351. https://doi.org/10.1016/j.watres.2016.07.059.

[16] E. Yamazaki, N. Yamashita, S. Taniyasu, J. Lam, P.K.S. Lam, H.B. Moon, Y. Jeong, P. Kannan, H. Achyuthan, N. Munuswamy, K. Kannan, Bisphenol A and other bisphenol analogues including BPS and BPF in surface water samples from Japan, China, Korea and India, Ecotoxicology and Environmental Safety. 122 (2015) 565–572. https://doi.org/10.1016/j.ecoenv.2015.09.029.

[17] G. Boczkaj, A. Fernandes, Wastewater treatment by means of advanced oxidation processes at basic pH conditions: A review, Chemical Engineering Journal. 320 (2017) 608–633. https://doi.org/10.1016/j.cej.2017.03.084.

[18] D.B. Miklos, C. Remy, M. Jekel, K.G. Linden, J.E. Drewes, U. Hübner, Evaluation of advanced oxidation processes for water and wastewater treatment – A critical review, Water Research. 139 (2018) 118–131. https://doi.org/10.1016/j.watres.2018.03.042.

[19] E. Brillas, I. Sirés, M.A. Oturan, Electro-fenton process and related electrochemical technologies based on fenton's reaction chemistry, Chemical Reviews. 109 (2009) 6570–6631. https://doi.org/10.1021/cr900136g.

[20] E. Brillas, A review on the photoelectro-Fenton process as efficient electrochemical advanced oxidation for wastewater remediation. Treatment with UV light, sunlight, and coupling with conventional and other photo-assisted advanced technologies, Chemosphere. 250 (2020). https://doi.org/10.1016/j.chemosphere.2020.126198.

[21] E. Brillas, C.A. Martínez-Huitle, Decontamination of wastewaters containing synthetic organic dyes by electrochemical methods. An updated review, Applied Catalysis B: Environmental. 166–167 (2015) 603–643. https://doi.org/10.1016/j.apcatb.2014.11.016.

[22] E. Brillas, Electro-Fenton, UVA Photoelectro-Fenton and Solar Photoelectro-Fenton Treatments of Organics in Waters Electro-Fenton, UVA Photoelectro-Fenton and Solar Photoelectro-Fenton Treatments of Organics in Waters Using a Boron-Doped Diamond Anode: A Review, 2014.

[23] P.J.M. Cordeiro-Junior, R. Gonçalves, T.T. Guaraldo, R. da Silva Paiva, E.C. Pereira, M.R. de V. Lanza, Oxygen reduction reaction: Semi-empirical quantum

mechanical and electrochemical study of Printex L6 carbon black, Carbon. 156 (2020) 1–9. https://doi.org/10.1016/j.carbon.2019.09.036.

[24] P.J.M. Cordeiro-Junior, M.S. Kronka, L.A. Goulart, N.C. Veríssimo, L.H. Mascaro, M.C. dos Santos, R. Bertazzoli, M.R. de V. Lanza, Catalysis of oxygen reduction reaction for H2O2 electrogeneration: The impact of different conductive carbon matrices and their physicochemical properties, Journal of Catalysis. 392 (2020) 56–68. https://doi.org/10.1016/j.jcat.2020.09.020.

[25] P. Betoni Momo, C. Pavani, M.S. Baptista, T.J. Brocksom, K. Thiago De Oliveira, Chemical transformations and photophysical properties of meso-tetrathienyl-substituted porphyrin derivatives, European Journal of Organic Chemistry. 2014 (2014) 4536–4547. https://doi.org/10.1002/ejoc.201402227.

[26] J. Moreira, V. Bocalon Lima, L. Athie Goulart, M.R.V. Lanza, Electrosynthesis of hydrogen peroxide using modified gas diffusion electrodes (MGDE) for environmental applications: Quinones and azo compounds employed as redox modifiers, Applied Catalysis B: Environmental. 248 (2019) 95–107. https://doi.org/10.1016/j.apcatb.2019.01.071.

[27] M.S. Kronka, F.L. Silva, A.S. Martins, M.O. Almeida, K.M. Honório, M.R. v. Lanza, Tailoring the ORR selectivity for H 2 O 2 electrogeneration by modification of Printex L6 carbon with 1,4-naphthoquinone: a theoretical, experimental and environmental application study , Materials Advances. 1 (2020) 1318–1329. https://doi.org/10.1039/d0ma00290a.

[28] W.R.P. Barros, T. Ereno, A.C. Tavares, M.R.V. Lanza, In Situ Electrochemical Generation of Hydrogen Peroxide in Alkaline Aqueous Solution by using an Unmodified Gas Diffusion Electrode, ChemElectroChem. 2 (2015) 714–719. https://doi.org/10.1002/celc.201402426.

[29] W.R.P. Barros, R.M. Reis, R.S. Rocha, M.R.V. Lanza, Electrogeneration of hydrogen peroxide in acidic medium using gas diffusion electrodes modified with cobalt (II) phthalocyanine, Electrochimica Acta. 104 (2013) 12–18. https://doi.org/10.1016/j.electacta.2013.04.079.

[30] R.M. Reis, R.B. Valim, R.S. Rocha, A.S. Lima, P.S. Castro, M. Bertotti, M.R.V. Lanza, The use of copper and cobalt phthalocyanines as electrocatalysts for the oxygen reduction reaction in acid medium, Electrochimica Acta. 139 (2014) 1–6. https://doi.org/10.1016/j.electacta.2014.07.003.

[31] J.F. Carneiro, F.L. Silva, A.S. Martins, R.M.P. Dias, G.M. Titato, Á.J. Santos-Neto, R. Bertazzoli, M.R.V. Lanza, Simultaneous degradation of hexazinone and diuron using ZrO2-nanostructured gas diffusion electrode, Chemical Engineering Journal. 351 (2018) 650–659. https://doi.org/10.1016/j.cej.2018.06.122.

[32] L.C. Trevelin, R.B. Valim, J.F. Carneiro, A. de Siervo, R.S. Rocha, M.R.V. Lanza, Using black carbon modified with NbMo and NbPd oxide nanoparticles for the improvement of H2O2 electrosynthesis, Journal of Electroanalytical Chemistry. 877 (2020). https://doi.org/10.1016/j.jelechem.2020.114746.

[33]   J.D. Baran, H. Grönbeck, A. Hellman, Analysis of porphyrines as catalysts for electrochemical reduction of O2 and oxidation of H2O, Journal of the American Chemical Society. 136 (2014) 1320–1326. https://doi.org/10.1021/ja4060299.

[34]   T. He, C. Zhang, G. Will, A. Du, Cobalt porphyrin supported on graphene/Ni (111) surface: Enhanced oxygen evolution/reduction reaction and the role of electron coupling, Catalysis Today. 351 (2020) 113–118. https://doi.org/10.1016/j.cattod.2018.10.056.

[35]   C.A. Martínez-Huitle, S. Ferro, Electrochemical oxidation of organic pollutants for the wastewater treatment: Direct and indirect processes, Chemical Society Reviews. 35 (2006) 1324–1340. https://doi.org/10.1039/b517632h.

[36]   L.A. Goulart, S.A. Alves, L.H. Mascaro, Photoelectrochemical degradation of bisphenol A using Cu doped WO 3 electrodes, Journal of Electroanalytical Chemistry. 839 (2019) 123–133. https://doi.org/10.1016/j.jelechem.2019.03.027.

[37]   V.M. Vasconcelos, I.M.D. Gonzaga, A.R. Dória, P.J.M. Cordeiro-Junior, M.R.V. Lanza, K.I.B. Eguiluz, G.R. Salazar-Banda, Effects of temperature and heating method on the performance of Ti/Ru0.25Ir0.25Ti0.50O2 anodes applied toward Bisphenol S removal, Electrochimica Acta. 364 (2020). https://doi.org/10.1016/j.electacta.2020.137273.

[38]   Y. Zhang, Z. Ni, J. Yao, Enhancement of the activity of electrochemical oxidation of BPS by Nd-doped PbO2 electrodes: Performance and mechanism, Water (Switzerland). 12 (2020). https://doi.org/10.3390/W12051317.

[39]   V.B. Lima, L.A. Goulart, R.S. Rocha, J.R. Steter, M.R.V. Lanza, Degradation of antibiotic ciprofloxacin by different AOP systems using electrochemically generated hydrogen peroxide, Chemosphere. 247 (2020). https://doi.org/10.1016/j.chemosphere.2019.125807.

[40]   H. Guo, H. Wang, Q. Wu, J. Li, Degradation and mechanism analysis of bisphenol A in aqueous solutions by pulsed discharge plasma combined with activated carbon, Separation and Purification Technology. 190 (2018) 288–296. https://doi.org/10.1016/j.seppur.2017.09.002.

[41]   Y. Guo, Q. Xue, K. Cui, J. Zhang, H. Wang, H. Zhang, F. Yuan, H. Chen, Study on the degradation mechanism and pathway of benzene dye intermediate 4-methoxy-2-nitroaniline: Via multiple methods in Fenton oxidation process, RSC Advances. 8 (2018) 10764–10775. https://doi.org/10.1039/c8ra00627j.

[42]   W.H.M. Abdelraheem, M.K. Patil, M.N. Nadagouda, D.D. Dionysiou, Hydrothermal synthesis of photoactive nitrogen- and boron- codoped TiO2 nanoparticles for the treatment of bisphenol A in wastewater: Synthesis, photocatalytic activity, degradation byproducts and reaction pathways, Applied Catalysis B: Environmental. 241 (2019) 598–611. https://doi.org/10.1016/j.apcatb.2018.09.039.

[43]   C. Luo, R. Hou, G. Chen, C. Liu, L. Zhou, Y. Yuan, UVC-assisted electrochemical degradation of novel bisphenol analogues with boron-doped

diamond electrodes: kinetics, pathways and eco-toxicity removal, Science of the Total Environment. 711 (2020). https://doi.org/10.1016/j.scitotenv.2019.134539.

[44] S.H. Farjana, N. Huda, M.A.P. Mahmud, Life cycle assessment of cobalt extraction process, Journal of Sustainable Mining. 18 (2019) 150–161. https://doi.org/10.1016/j.jsm.2019.03.002.

[45] IARC Working Group on the Evaluation of Carcinogenic Risks to Humans., World Health Organization., International Agency for Research on Cancer., Cobalt in hard metals and cobalt sulfate, gallium arsenide, indium phosphide, and vanadium pentoxide, International Agency for Research on Cancer, 2006.

[46] M. Behl, M.D. Stout, R.A. Herbert, J.A. Dill, G.L. Baker, B.K. Hayden, J.H. Roycroft, J.R. Bucher, M.J. Hooth, Comparative toxicity and carcinogenicity of soluble and insoluble cobalt compounds, Toxicology. 333 (2015) 195–205. https://doi.org/10.1016/j.tox.2015.04.008.

[47] L. Leyssens, B. Vinck, C. van der Straeten, F. Wuyts, L. Maes, Cobalt toxicity in humans—A review of the potential sources and systemic health effects, Toxicology. 387 (2017) 43–56. https://doi.org/10.1016/j.tox.2017.05.015.

[48] R. Ortega, C. Bresson, C. Darolles, C. Gautier, S. Roudeau, L. Perrin, M. Janin, M. Floriani, V. Aloin, A. Carmona, V. Malard, Low-solubility particles and a Trojan-horse type mechanism of toxicity: The case of cobalt oxide on human lung cells, Particle and Fibre Toxicology. 11 (2014) 1–18. https://doi.org/10.1186/1743-8977-11-14.